EFFECT OF PROJECTILE TYPE, SIZE AND IMPACT VELOCITY ON BALLISTIC IMPACT FAILURE BEHAVIOR OF TROGAMID® CX-7323 NYLON

Nicholas Tsantinis*, John W. Song
US ARMY NSRDEC, AMSRD-NSR-WS-DB Natick, MA. 01760

Roy Paulson
Paulson MFG. Co., Temecula, CA 92592

ABSTRACT

Extensive study on the fracture behavior of TROGAMID® CX-7323 (CX-7323) nylon under ballistic impact was performed. Generally, CX-7323 exhibits ductile failure upon impact with a 17-grain fragment simulating projectile(s) (FSP). Penetration is initiated by ductile shearing upon impact. Subsequent tensile stretching allows the penetration event to progress. Material in front of the projectile is pushed out of the way during penetration. Significant elastic recovery of the exit hole is noticed after complete penetration. Upon impact of a right circular cylinder(s) (RCC) the failure behavior was mixed depending on the size of the fragment. With smaller RCC (2-grain, 4-grain) the failure is similarly ductile as when impacted with FSP. Larger RCC (16-, 17- and 64-grain) at impact velocities above the ballistic limit frequently cause a different failure mode in CX-7323 nylon. Initial penetration is marked by ductile shearing with a hole similar in size to the projectile. Upon complete penetration, brittle, conoid spallation occurs.

Annealing negatively affected notched Izod impact results, but ballistic performance was maintained past temperatures significantly higher than the Glass Transition (T_g) of CX-7323.

1. INTRODUCTION

Transparent armor is an important frontier in the arena of personnel protection. Over the course of several decades polycarbonate has remained the material of choice with regards to transparent personnel armor. With good fragment resistance, easy manufacturability and relatively low cost this has proven the best option. Recently, significant efforts have been focused on a transparent thermoplastic nylon, CX-7323 [1]. CX-7323 is a permanently transparent, high strength polymer with excellent chemical resistance [2].

Material failure studies have been performed that correlate failure behavior to projectile nose type [3-5]. Børvik et al. [3] observed three different types of perforation failure in steel plates upon impact of three types of projectiles. They noticed that impact by blunt-nosed projectiles caused failure by plugging of the steel plate. Conical projectiles caused bulging followed by petalling of the distal face of the target. Hemispherical projectiles exhibited failure in between the former two.

Wright et al. [5] observed various modes of failure in Polycarbonate upon impact with differently shaped projectiles. Spherical missiles tended to cause final failure by petalling. Cylindrical projectiles exhibited different failure types depending on material thickness. At lower plate thicknesses, failure was exhibited by a domed cap. Thicker samples failed via shear plugging.

The two aforementioned studies come to different conclusions regarding projectile shape and its effect on ballistic limit. Børvik [3] noticed a significant difference in the ballistic limit of steel plates impacted by blunt projectiles compared to those impacted by hemispherical and conical missiles. Wright [5] noticed no difference in the ballistic limit of polycarbonate when impacted by spherical or blunt projectiles.

Song et al. [1, 6] noticed different failure behavior of PolyMethylMethacrylate (PMMA) at different thicknesses and striking velocities. At lower thicknesses and velocities, PMMA exhibits catastrophic, brittle failure with nearly no energy absorption. At higher thicknesses and striking velocities, localized micro-cracking around the impact area is the dominant failure mode. This increases energy absorption and consequently raises the ballistic limit [1, 6].

2. EXPERIMENTAL

2.1 Projectiles

Ballistic testing was conducted against two main types of fragments; FSP and RCC. The FSP is a small cylinder with an ogive, chiseled nose possessing a chisel angle of 35º. It has a nominal weight of 1.10 grams and a diameter of .22 caliber. The RCC differs from the FSP in that it has a blunt nose. Testing against the RCC utilized five different sizes including 2-grain, 4-grain, 16-grain, 17-grain and 64-grain.

2.2 Test Samples

CX-7323 polymer was purchased from Evonik Degussa, Inc. Test samples were prepared by Paulson MFG. by injection molding of 152.4 mm square flat plates with various thicknesses. Sample thicknesses examined in this study were 6.35 mm and 3.175 mm.

2.3 Annealing

76.2 mm square samples of 6.35 mm and 3.175 mm thickness were given a heat treatment. Samples were heated to three different temperatures (100°C, 130°C, 150°C) and exposed for three different times (30min, 60min, 120min). A Blue M electric convection oven was set to reach these temperatures within a 15minute ramp time. Oven and sample temperatures were monitored with thermocouples. A MATLAB model was devised, based on the First Law of Thermodynamics to predict temperature rise within the samples.

2.4 Izod Impact

Izod impact tests were performed on samples using a BPI izod impact tester according to ASTM D-256. Rectangular samples measuring 6.35 mm x 12.7 mm, and of notch width 6.35 mm and 3.175 mm were tested. A TMI notch cutter was used to notch samples prior to pendulum impact. A hammer with a maximum energy output of 5.42 J was used to strike the samples.

2.5 Ballistic Evaluation

For ballistic evaluations against 17-grain FSP and 17-grain RCC, a high-velocity impact test apparatus at NSRDEC was utilized. Samples cut to approximately 76.2 mm square were mounted between two aluminum plates. Each plate had four 50.8 mm diameter circular openings at each corner. This sample holder was then clamped in the center of the high-velocity impact test apparatus.

A single-stage, helium powered gas gun with a barrel length of 0.8 m was used to propel projectiles. Because of its high speed of sound, helium is a favorable propellant for use in gas gun applications as it can easily achieve relatively high muzzle velocities. Velocities were controlled via variable input pressure using previously configured calibration curves. Firing was controlled using an electric solenoid valve.

Ballistic evaluations against 2-, 4-, 16- and 64-grain RCC were performed at H. P. White Laboratories, Inc. Street, MD. All tests at both locations (NSRDEC and H.P. White) were conducted in accordance with the procedures of MIL-STD-662F [7].

3. RESULTS AND DISCUSSIONS

3.1 Effect of projectile types and sizes

In this study, ballistic testing was conducted against two main types of fragments; the Fragment Simulating Projectile (FSP) and the Right Circular Cylinder (RCC).

Figure 1 exhibits the typical failure deformation at striking velocity below that required for complete penetration. Ductile shearing is followed by tensile stretching and bulging at the target's back face. In the absence of complete penetration, the failure progression is arrested here and remains ductile. Such behavior was observed upon impact of both FSP and RCC projectiles.

Figure 2 presents an example of brittle failure observed during ballistic impact. A conoidal spall is ejected from the target. Circumferential cracking is the dominant visible artifact of this failure, with substantial radial cracking also present.

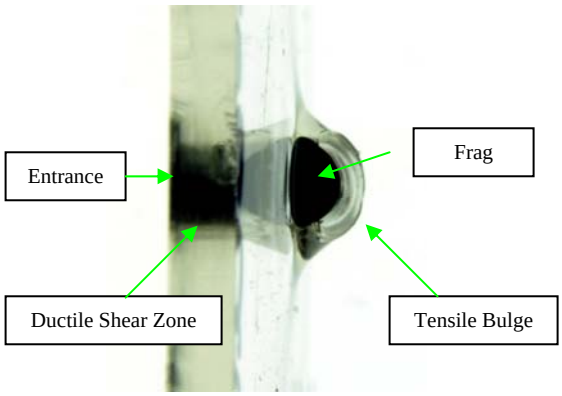

Figure 1. Typical failure deformation exhibited by CX-7323 nylon at striking velocity lower than required for complete penetration. The fragment is captured within the bulged plastic.

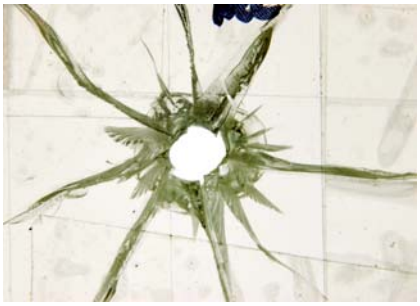

Figure 2. Brittle Failure observed from the impact of blunt nosed 17-gr. RCC.

Figures 3, 4 and 5 exhibit that samples tested against the FSP generally exhibited ductile failure. For both FSP

and RCC impact, failure deformation during partial penetrations is similar to that illustrated in Figure 1.

Typical ductile failure upon complete penetration of an FSP is shown in Figure 3. Upon impact, penetration begins via ductile shearing; A void about the diameter of the projectile progresses partially through the thickness of the sample. Following this, tensile stretching occurs as evident in the stretched zone near the projectile exit hole.

As shown in Figure 4, stress whitening, presumably due to friction effects is prevalent around the exit zone. Thinning in front of the projectile dominated target failure, with material ahead of the fragment being pushed out of the way. Upon complete penetration, a small plug is ejected from the sample as shown in Figure 5. This plug is of varying thickness, and decreases in diameter closer to the back face of the target. After complete penetration, elastic recovery of the exit hole occurs. The hole diameter reduces significantly to much smaller than the projectile diameter. This is evident in Figure 3 and is labeled as such.

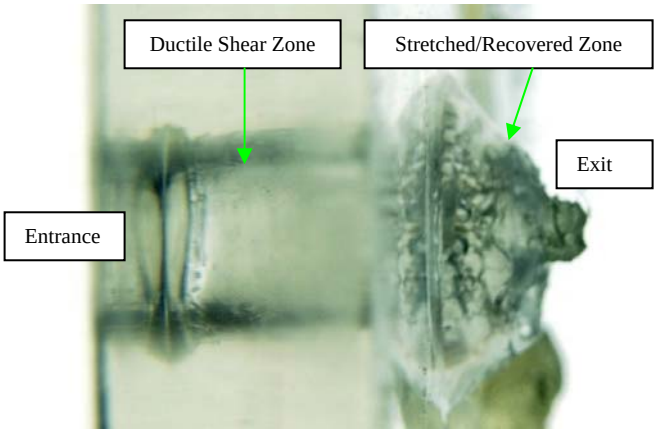

Figure 3. Typical Ductile Perforation Failure (FSP impact)

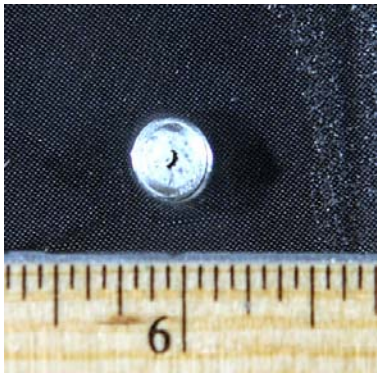

Figure 4. Stress Whitening shown after the penetration of an FSP.

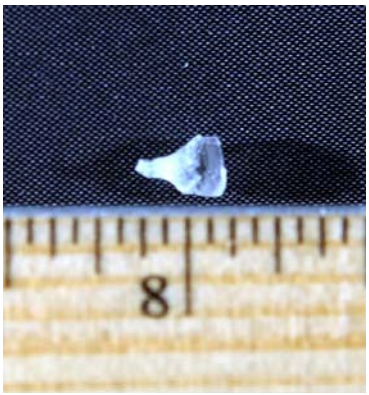

Figure 5. Tapered Plug generated during ductile penetration of an FSP.

Failure behavior with blunt nosed RCC fragments was mixed. The 2-grain RCC generally exhibited ductile failure similar to that shown upon impact with an FSP. In some instances where the striking velocity was well above the ballistic limit, minor cracking did occur, but was absent of significant spallation.

The 4-grain RCC also showed mostly ductile failure. All partial penetrations failed ductally, while most complete penetrations did as well. As exhibited in some 2-grain samples, some minor cracking is evident at striking velocities well above the ballistic limit. Since there was no spallation from the exit face, this may be due to the extremely close proximity of some shots to one another.

However, the blunt nosed 16-, 17- and 64-grain RCC frequently exhibited brittle fracture upon complete penetration. A brittle conoidal spall is ejected from the backface of the sample at striking velocities above the ballistic limit. Although brittle fracture was the end result, the impacted areas show evidence of ductile deformation. Ductile shearing, as described in the fracture behavior of FSP occurs in this case as well. Conoid spallation of the exit area occurred after the initial ductile deformation. Figure 6 shows the conoidal spall from the exit area. As can be seen, the projectile is still in the fractured piece, which is clear evidence of initial ductile failure of this material upon ballistic impact, followed by subsequent brittle spallation.

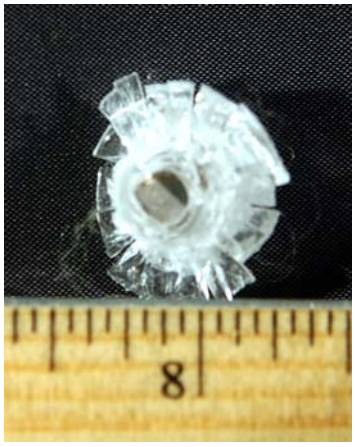

Figure 6. Conoid Spall with Intact projectile upon complete penetration of RCC.

3.2 Effect of projectile velocity and impact obliquity angle

Brittle failure behavior was also observed at high velocities significantly above the V_{50} ballistic limit for some fragment sizes. Most of the brittle fractures were observed at 0° impact obliquity. At 45° impact obliquity, CX-7323 nylon exhibited ductile failure and showed stress whitening (see Figure 7).

Figure 7. Ductile failure observed on 45° obliquity angle impact of 16-grain RCC.

Figure 8 exhibits the brittle failure typical of impact with larger caliber RCC. Some circumferential cracking is noticed in the fractured area. A chunk, much larger than the diameter of the projectile is spalled out the back of the sample.

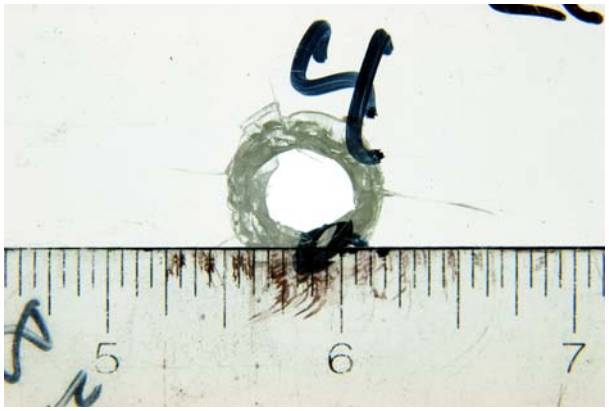

Figure 8. Brittle failure observed on 0° obliquity angle impact of 16-grain RCC.

The 17-grain RCC results were not as conclusive as seen with 16-grain. Frequently, spallation did occur out the back face of the sample, but ductile failure occurred frequently upon complete penetration as well. As evident in Figure 2, typical brittle failure exhibited radial cracking across the width of the target. More detailed examination of the failure behavior of 16-grain and 17-grain RCC is currently underway.

The 64-grain RCC exhibited failure similar to the 16-grain projectile. Figure 9 exhibits severe spallation in the case of 0° impact obliquity. As seen in Figure 10, in the 45° obliquity case, much of the material is pushed out of the way. Whitening is evident on the back face of the sample, indicating significant ductile deformation during perforation.

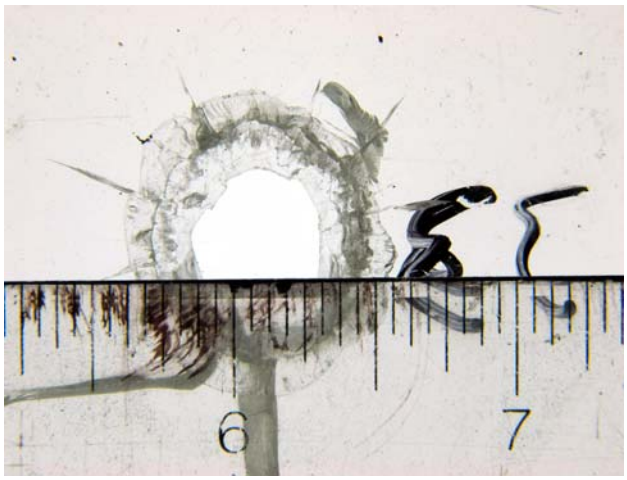

Figure 9. Brittle failure observed on 0° obliquity angle impact of 64-grain RCC.

Figure 10. Ductile failure observed on 45° obliquity angle impact of 64-grain RCC.

3.3 Effect of annealing

To further examine the cause of the occasional brittle fracture behavior, a preliminary study on annealing of the injection molded CX-7323 nylon was performed. The possible presence of built-up residual stress from the injection molding process was evaluated through annealing. CX-7323 Nylon samples were annealed at three different temperatures in an electric convection oven and subsequently tested against the two fragment types (17-grain). Samples were annealed at 100°C, 130°C and 150°C for 30minutes, 60 minutes and 120 minutes each. Figure 10 exhibits the typical annealing profile of the 6.35 mm thick samples. Shown are thermocouple readouts from the oven (red) and actual sample (blue). The figure also shows that the time lag between the equilibrium of sample temperature and oven temperature is quite small.

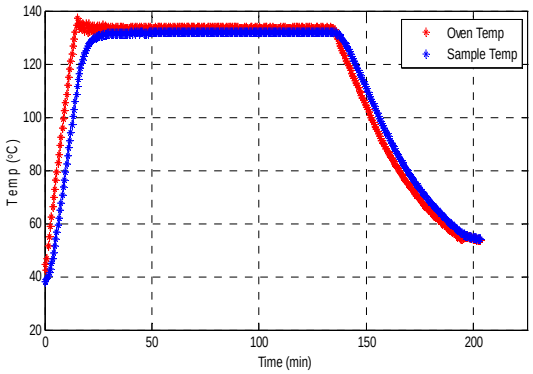

Figure 10. Typical Annealing Profile of 6.35 mm CX-7323 nylon.

Figure 11 exhibits the ramping profile of the 6.35 mm thick samples. A MATLAB model based on the 1st Law of Thermodynamics predicts the temperature ramp in the sample. Predictions matched measured values very well.

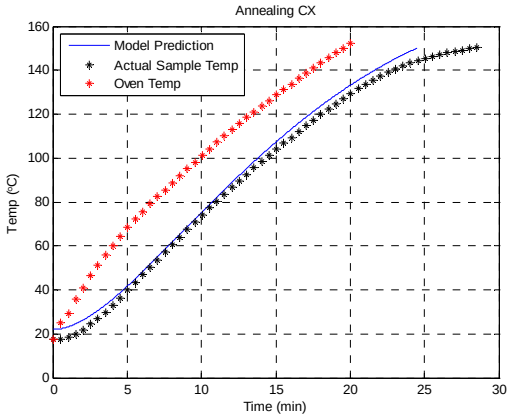

Figure 11. Comparison between measured and predicted ramping temperatures.

Visual observation of samples exposed to 100°C and 130°C generally did not show significant evidence of degradation. However, those samples exposed to 150°C exhibited cloudiness as well as occasional warping.

Table 1 exhibits the ballistic performance of CX-7323 before and after annealing. In all cases, samples annealed at 150ºC exhibit significantly lower V_{50} values and brittle fracture. Some of these samples were so physically distorted due to the heat treatment they were not tested.

For 6.35 mm thick samples, ballistic performance of FSP and RCC show noticeable differences. In the case of FSP impact, the V_{50} ballistic limit did not change significantly for 100ºC and 130ºC treatments. However, in the case of RCC impact, the V_{50} ballistic limit starts to drop noticeably beginning with the 130ºC 30 minutes annealing treatment.

For 3.175 mm thick samples, ballistic performance did not deteriorate until 130ºC 120 minutes annealing treatment. An interesting note to mention here is that the izod impact strength of 3.175 mm samples listed in the table shows a significant drop from the un-annealed control samples. The level of notch sensitivity now shown in 3.175 mm samples is similar to that commonly shown in 6.35 mm control samples. These results suggest that the notch sensitivity of the material does not directly affect the ballistic failure behavior.

3.4 Izod Impact

Wolstenholme et al. [8] noticed sensitivity in the failure strength of polycarbonate under izod impact. Samples with notch width below 6.35 mm exhibited a drastic increase in impact strength. In this study, notch sensitivity was also noticed in CX-7323 nylon as shown in Figure 12 and Table 1.

.

Table 1. Effect of annealing conditions on izod impact strength and V_{50} ballistic limits with 17-grain FSP and RCC.

Annealing Treatment		6.35 mm			3.175 mm		
		Izod Impact Strength (J/m)	*V_{50} (m/s) FSP*	*V_{50} (m/s) RCC*	*Izod Impact Strength (J/m)*	*V_{50} (m/s) FSP*	*V_{50} (m/s) RCC*
Control (No Heat Treatment)		130	344	343	1077	254	248
100°C	*30 min*	102	335	333	147	248	248
	60 min	107	330	325	134	247	259
	120 min	101	330	318	128	256	248
130°C	*30 min*	109	329	309	115	251	234
	60 min	92.4	334	314	101	254	258
	120 min	96.7	329	---	78.7	173	191
150°C	*30 min*	52.9	---	---	58.4	117	123
	60 min	58.5	---	---	51.9	124	110
	120 min	55.4	---	---	51.9	114	109

--- indicates data point not taken due to excessive sample distortion

As notch width increases from 3.175 mm to 6.35 mm, the failure mode changes from a hinge break with ductile necking at the notch to a complete break brought on by shear failure. This suggests that the preferred mode of energy absorption during the notched izod impact is necking at the notched area (see Figure 13). However, as mentioned in the previous section and shown in Figure 12 and Table 1, the annealing process changed the mode of failure from necking to brittle shear failure even on 3.175 mm samples. This suggests that molecular relaxation from the annealing process, even at T_g or at temperatures lower than T_g, actually increased the notch sensitivity of CX-7323.

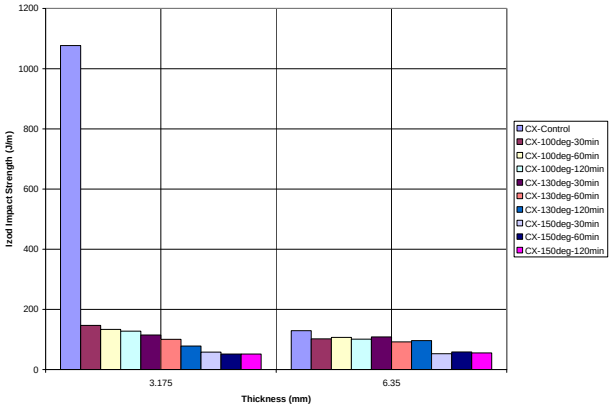

Figure 12. Izod impact strength of annealed and control CX-7323 samples.

Figures 14 and 15 exhibit results of scanning electron microscopy studies of the izod samples. Necking is visible in the 3.175 mm sample, while not present in the 6.35 mm sample. Both micrographs show significant plastic flow along the failure face.

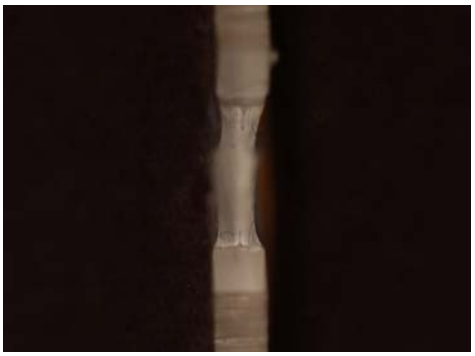

Figure 13. Necking of notched area on thin (3.175 mm) Izod sample.

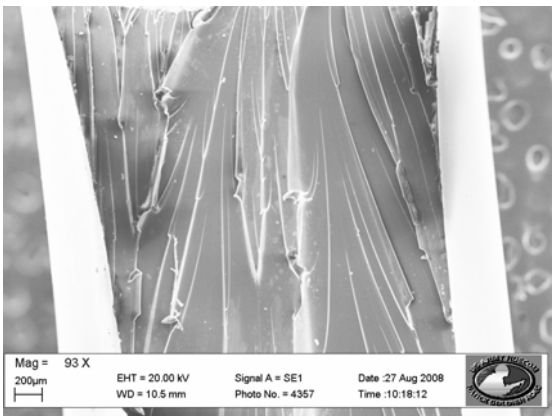

Figure 14. Scanning electron micrograph of 3.175 mm CX-7323 upon Izod impact failure.

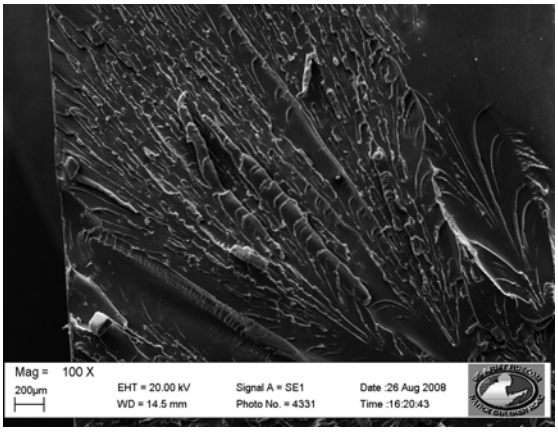

Figure 15. Scanning electron micrograph of 6.35 mm CX-7323 upon Izod impact failure.

CONCLUSIONS

The fracture behavior of CX-7323 upon ballistic impact was examined. It seems that the fracture behavior of CX-7323 is affected by the type or shape of the projectile. Generally, the failure upon impact of an FSP is ductile in nature. However, upon impact with blunt nosed RCC, the fracture behavior of CX-7323 was mixed. Both ductile failure as well as brittle fracture were observed.

The size of the projectile also affected the fracture behavior of CX-7323. For RCC, 2- and, 4-grain sizes showed ductile failure similar to that shown with 17-grain FSP. However, failure modes observed on 16-, 17- and 64-grain RCC showed more occurrences of brittle than ductile failure.

Velocity and angle of incidence also influenced the failure behavior of CX-7323. At velocities, significantly higher than the ballistic limit, occasional brittle failures were observed even with small projectiles. However, all brittle fracture observed in this study occurred when the samples were tested at 0° impact obliquity. All samples shot at 45° impact obliquity exhibited ductile behavior.

Moreover, brittle fracture accompanies the ductile mode of failure along the path of the projectile by exhibiting ductile stretching with shearing through the path of the projectile. Brittle fracture occurs after or just before the exit of the projectile. Brittle failure only occurred upon complete penetration. This suggests that most of the energy absorption might be from the ductile passage of the projectile. Therefore, the velocity required for brittle failure is generally around or above the V_{50} region.

Annealing effects on the fracture behavior were also examined. Annealing at temperatures below the glass transition temperature (T_g) and around T_g did not show significant deterioration of ballistic performance or fracture behavior. However, above T_g, evidence of crystallization of CX-7323 was clear and exhibited by visible cloudiness. Furthermore, some samples annealed at temperature above T_g were warped.

Notched izod impact strength showed significant sensitivity, especially on 3.175 mm samples. Upon annealing, ductile CX-7323 3.175 mm samples exhibited brittle failure similar to 6.35 mm CX-7323. This indicates that the molecular structural stability imposed via molecular relaxation upon annealing reduced the ductility and created notch sensitivity as shown with thicker samples (6.35 mm).

Greater notch sensitivity of already poorly performing 6.35mm samples was evident through noticeable reduction of the izod impact strength of annealed samples as the annealing conditions became harsher.

AKNOWLDEGEMENTS

The authors would like to thank Dave Ziegler at NSRDEC for his invaluable assistance with Scanning Electron Microscopy of test samples.

REFERENCES

1. Song John W., et al. “Aromatic Nylons for Transparent Armor Applications.” Proceedings 25th Army Science Conference (2006)
2. Degussa TROGAMID® CX-7323 Technical Brochure
3. Børvik T, et al. “Perforation of 12mm thick steel plates by 20 mm diameter projectiles with flat, hemispherical and conical noses Part I: Experimental study.” International Journal of Impact Engineering 27 (2002) 19-35.
4. Wilkins Mark, L. “Mechanics of Penetration and Perforation” International Journal of Engineering Science. 16 (1978) 793-807
5. Wright S.C., et al. “Ballistic Impact of Polycarbonate-An Experimental Investigation.” International Journal of Impact Engineering 13 (1993) 1-20
6. John W. Song and Alex J. Hsieh, “Ballistic Impact Resistance of Monolithic, Hybrid and Nano Composites of PC and PMMA”, Proceedings of the American Society for Composites 17th Technical Conference (2002)
7. MIL-STD-662F, “Department of Defense Test Method Standard V50 Ballistic Test For Armor” (1997)
8. Wolstenholme W.E., et al. “Factors Influencing Izod Impact Properties of Thermoplastics Measured with the Autographic Impact Test.” J. of Applied Polymer Science. 8 (1964) 119-140